Biomaterials and Biosystems 8 (2022) 100064

Contents lists available at ScienceDirect

Biomaterials and Biosystems

journal homepage: www.elsevier.com/locate/bbiosy

Polycaprolactone-collagen nanofibers loaded with dexamethasone and simvastatin as an osteoinductive and immunocompatible scaffold for bone regeneration applications

Hilal Ahmad Rather[a], Johnna Francis Varghese[b], Bindiya Dhimmar[a], Umesh C.S. Yadav[c], Rajesh Vasita[a,*]

[a] Biomaterials & Biomimetics Laboratory, School of Life Sciences, Central University of Gujarat, Gandhinagar, 382030, India
[b] School of Life Sciences, Central University of Gujarat, Gandhinagar, 382030, India
[c] Metabolic Disorders and Inflammatory pathologies Laboratory, Special Centre for Molecular Medicine, Jawaharlal Nehru University, New Delhi, 110067, India

ARTICLE INFO

Keywords:
Dual drug delivery
Macrophage
Anti-inflammatory
Mesenchymal stromal cells
Osteogenesis
Bone regeneration

ABSTRACT

Physiological inflammation has been shown to promote bone regeneration; however, prolonged inflammation impedes the osteogenesis and bone repair process. To overcome the latter we aimed to develop a dual drug delivering nanofibrous scaffold to promote osteogenic differentiation of mesenchymal stromal cells (MSCs) and modulate the pro-inflammatory response of macrophages. The polycaprolactone (PCL)-collagen nanofibrous delivery system incorporating dexamethasone and simvastatin was fabricated by electrospinning process. The morphological analysis and mRNA, as well as protein expression of proinflammatory and anti-inflammatory cytokines in human monocytes (U937 cells), demonstrated the immunocompatibility effect of dual drug-releasing nanofibrous scaffolds. Nitric oxide estimation also demonstrated the anti-inflammatory effect of dual drug releasing scaffolds. The scaffolds demonstrated the osteogenic differentiation of adipose-derived MSCs by enhancing the alkaline phosphatase (ALP) activity and mineral deposition after 17 days of cell culture. The increased expression of Runt-related transcription factor-2 (RUNX-2) and osteocalcin at mRNA and protein levels supported the osteogenic potential of dual drug-loaded fibrous scaffolds. Hence, the results indicate that our fabricated nanofibrous scaffolds exhibit immunomodulatory properties and could be employed for bone regeneration applications after further in-vivo validation.

1. Introduction

In-situ bone tissue engineering utilizes a variety of scaffolds functionalized with osteoinductive factors. Controlled release of the osteoinductive growth factors from bioactive scaffolds, for instance, bone morphogenetic proteins can regenerate the bone defect [1]. However, their applications are limited due to their shorter half-life and the interaction of immune cells with the scaffolds [2,3]. Further, chronic inflammation inhibits the bone repair process which leads to delayed healing and non-union of bone defects [4]. Several studies focused on engineering biomaterials to create a microenvironment that suppresses proinflammatory responses and promotes bone repair and regeneration. These scaffolds strive to achieve immunomodulation through various mechanisms, such as changing the physical property of biomaterials, alteration of surface chemistry and controlled release of immunomodulatory molecules [5]. Due to the presence of chronic inflammation, activation of recruited macrophages is skewed towards the M1 phenotype, and their prolonged presence reduces the inherent potential of bone regeneration. However, their transition towards the alternative M2 phenotype is associated with tissue homeostasis restoration, scaffold integration, and acceleration of the bone regeneration process [6]. The M2 polarization facilitates the immune compatibility of the scaffold and supports osteogenesis as well. Recently studies by Dai et al. and Manhon et al. have demonstrated the improvised bone regeneration by modulating macrophage from M1 to M2 phenotypes [7,8]. Hence, it is desirable to create a scaffold that could polarize the macrophages and promotes the osteogenesis.

The extracellular matrix contains bioactive domains that bind to immune cell receptors and regulate their functions [9]. ECM proteins have been utilized to fabricate biomaterial scaffolds to mimic the natural regulatory role of the matrix for immunomodulation purposes [5]. In this context, polycaprolactone (PCL) a biodegradable polymer mixed with collagen type 1 was utilized to fabricate ECM mimicking nanofibrous scaffold. PCL is an FDA approved polymer, which is extensively used as implantable biomaterial for controlled release of drugs [10]. Furthermore its osteogenic functionality is increased by adding certain biopoly-

* Corresponding author.
E-mail address: rajesh.vasita@cug.ac.in (R. Vasita).

https://doi.org/10.1016/j.bbiosy.2022.100064
Received 16 April 2022; Received in revised form 25 September 2022; Accepted 26 September 2022

mers in electrospinning solution, for instance, chitosan, gelatin, collagen [11–13]. Dexamethasone, a well-known glucocorticoid with anti-inflammatory properties, through its prolonged and controlled release from scaffolds has been shown to direct the macrophage polarization to M2 phenotype along with suppressing the inflammatory pathways [14]. It is also utilized as a principal component for osteogenic differentiation media as it induces osteogenesis in mesenchymal stromal cells (MSCs) by increasing bone morphogenetic protein-2 [15]. Simvastatin is a cholesterol-lowering drug and is also known for its pro-angiogenic role. It enhances bone mineralization, alkaline phosphatase activity along with increasing the expression of osteocalcin, sialoprotein, and type I collagen in bones [16]. Further, it is known to block the RANKL-induced osteoclastogenesis and is also reported to induce osteogenesis in MSCs [17]. However, there are scant studies about the immunomodulation of scaffolds fabricated with simvastatin.

Therefore, in this study, we have fabricated an osteoconductive and osteoinductive scaffold that can enhance the biological process of bone regeneration and modulate immune response. The dual drug loaded PCL-collagen nanofibrous scaffolds was fabricated by electrospinning, and characterrized for its osteogenic potential and immunocompatibility.

2. Materials and methods

2.1. Materials

PCL (average Mn 8000 Da), 4-Nitrophenyl, phorbol 12-myristate 13-acetate (PMA) alizarin red, dexamethasone, and resazurin were purchased from Sigma Aldrich, USA. Collagen type 1 was isolated and purified in house from rat tails tendons (kindly provided by Flair Lab, Surat. India) following the reported protocol [18]. Hexafluoro-2-propanol was obtained from Chemsworth, India, and simvastatin from Enzo Life Sciences, India. The cDNA synthesis kit was procured from Clontech Takara, USA whereas the RNA-isolation kit and PCR master mix were purchased from Macherey-Nagel, Germany, and Thermo Fisher Scientific, USA respectively. Primers for selective genes were purchased from Imperial Life Sciences, India. Cy3 conjugated antibodies for Runt-related transcription factor-2 (RUNX2) and Osteocalcin were purchased from Bioss antibodies, USA. Predesigned cytokine testing ELISA kit was procured from Qiagen, Hilden, Germany. Adipose-derived mesenchymal stromal cells at passage 1, HiMesoXL^{TM} MSC Expansion Medium, HiMesoXL^{TM}, and MSC Growth Supplement, were purchased from HiMedia, India.

2.2. Scaffold fabrication

Nanofibrous scaffolds were fabricated from PCL and collagen type 1 by electrospinning process. 5% of PCL and collagen in a 1:1 ratio was solubilized overnight in 1,1,1,3,3,3, Hexafloro-2-propanol (HFIP) and utilized for the fabrication of nanofibrous scaffolds. For drug-loaded scaffolds, 100 μg of each of dexamethasone and simvastatin was loaded separately or in combination with the polymeric solution before electrospinning. The polymeric solution was dispensed at 50 μl/min with 15 cm distance between electrodes and under the electric field strength of 25 kV. The scaffolds were lyophilized and stored at −20 ˚C for further experimental procedures.

2.3. Scaffold morphology analysis

A scanning electron microscope (SEM) (EVO 18, Zeiss, Germany) was used to observe the morphological features of electrospun fibers. Briefly, the lyophilized scaffolds were sputter-coated with gold-palladium. SEM imaging of the scaffolds was performed at 10 to 15 kV with varying distances (10 to 20 mm) between sample and electron source.

2.4. Scaffold wide-angle X-ray diffraction (XRD) analysis

XRD analysis was carried out to study the crystal structure level of polymers after drug encapsulation and electrospinning. The analysis was performed using a wide-angle x-ray diffractometer (D8 discover, Bruker, USA). At 40 kV and 30 mA, the X-rays were generated whereas the scan was performed from 5˚ to 50˚ at the rate of 0.05˚ increment/step with a scan speed of 0.2 s/step. The grazing angle was kept 2˚ for analysis of thin film of PC (PCL-collagen scaffold), PCD (PC + dexamethasone), PCS (PC + Simvastatin), PCDS (PC + dexamethasone + Simvastatin), and PCL film. All the measurements were recorded at an ambient temperature.

2.5. Scaffold degradation analysis

The fiber degradation was carried out at physiological pH, in phosphate-buffered saline (PBS). Briefly, five samples for each time point from PC and PCDS with dimensions of 1 cm^2 and 0.5 cm^2 were lyophilized, and dry weight of each sample was measured. The samples were incubated in 1 ml of PBS and kept in a shaking water bath at 37 ˚C and 20 rotations per minute (RPM). PBS was changed twice a week and samples were terminated on 7th, 14th, and 28th days. Afterward, samples were lyophilized and the dry weight of samples was measured. Finally, the images were recorded by SEM analysis, as mentioned in Section 2.3.

2.6. In-vitro immunomodulation study

Human monocytes (U937 cells) procured from ATCC (Manassas, VA, USA) were utilized for immunomodulation study at passage 17 to 19. The cells were cultured in RPMI 1640 media with 1% antibiotic and 10% fetal bovine serum obtained from Gibco Life Technologies (Grand Island, NY, USA). Media was replaced every alternate day. For experiments, 1×10^5 U937 cells were seeded on each prepared scaffold and cultured for 48 hour (h). For control, cells were cultured on tissue culture polystyrene surface (TCPS) and for the positive control, the cells were treated with 15 nM PMA before seeding.

2.7. Cell morphological studies

Change in the cell morphology of monocytes and differentiation to macrophages is attributed to the pro-inflammatory response. The cells were grown for 48 h as mentioned above and their morphological analysis was carried out using SEM. Briefly, cells were fixed using 2% glutaraldehyde in 0.1 M sodium cacodylate buffer (pH7.2) for 1 h. The samples were then subjected to dehydration using gradient ethanol series. Samples were air-dried and lyophilized overnight. The SEM imaging was performed as mentioned in Section 2.3. The cell morphological features were calculated as reported earlier [19] in ImageJ using the following formula

$$\text{Circularity} = 4\pi\times(\text{Area}/\text{Perimeter})^2$$

The value of 1.0 indicates a perfect circle. As the value approaches 0.0, it indicates an increasingly elongated shape. The aspect ratio was calculated as

$$\text{Aspect ratio} = \text{Major axes}/\text{Minor axes}$$

2.8. Nitric oxide estimation

Production of nitric oxide (NO) by monocytes and macrophages is attributed to the pro-inflammatory phenotype. Nitrite produced by oxidization of NO is assessed to determine the amount of NO produced. 1×10^5 U937 cells were seeded on each scaffold and PMA induced monocytes were taken as a positive control. After 48 h of incubation, 100 μl of the media supernatant was collected from each group and mixed with 100 μl of Griess reagent. After 30 min of incubation at room

temperature (RT), the absorbance was measured at 548 nm using a Synergy H1 Hybrid microplate reader.

2.9. Gene expression study

The expression level of pro-inflammatory and anti-inflammatory markers were studied at the mRNA level by performing qPCR. Briefly, total RNA was isolated from the U937 cells grown on the different scaffolds. RNA was isolated using NucleoSpin® RNA isolation kit and the procedure was followed as per the manufacture's protocol. RNA was quantified using Nano drop method in UV–Visible spectrophotometer (Synergy H1, BioTek Instruments, USA). 1 μg RNA from each sample was reverse transcribed to cDNA in 20 µl reaction mix using PrimeScript™ 1st strand cDNA synthesis kit (Takara, Japan). Primers for selected genes such as IL-1β (F: 5′CCTGTCCTGCGTGTTGAAAG 3′ R: 5′GGGAACTGGGCAGACTCAAA 3′, IL-10 (F: 5′CTGAGAACCAAGACCCAGACA3' R: 5′AAAGGCATTCTTCACCTGCTCC 3′), GM-CSF (F: 5′CCGGAAACTTCCTGTGCAAC 3′ R: GTCTCACTCCTGGACTGGCT 3′), TNF-α (F: 5′ CGAGTGACAAGCCTGTAGCC 3′, R: 5′ GGACCTGGGAGTAGATGAGGT3') and normalized using GAPDH (F: 5′GCCTTCCGTGTCCCCACTGC3' R: 5′ CAATGCCAGCCCCAGCGTCA 3′) were obtained from Eurofins (Brussels, Belgium). A total reaction mixture of 20 µl was set up for qPCR containing 2X SYBR green mix and 1 µl of cDNA. PCR was carried out in optical microamp 96-well reaction plate using AB-7500 PCR machine.

Osteogenic differentiation of MSCs on different fibrous scaffolds were also characterized at molecular level by performing mRNA expression study. RNA isolation and cDNA synthesis from MSCs was performed as above. 20 µg reaction mix was used for PCR with following primers were used RUNX 2 (F: 5′TTACTTACACCCCGCCAGTC 3′, R: TATGGAGTGCTGCTGGTCTG 3′, osteocalcin (F: GACTGTGACGAGTTGGCTGA 3′, R: GGAAGAGGAAAGAAGGGTGC 3′ and normalized with GAPDH (F: 5′TGCACCACCAACTGCTTAG 3′ R: 5′GGATGCAGGGATGATGTTC 3′). The PCR was set for 35 cycles. Final product was mixed with 6X DNA loading dye and run in 1.5% agarose gel. Bands were captured using Gel doc imaging system (Syngene, G:BOX, UK) and the bands densities were quantified using Alpha Imager software (San Jose, CA, USA).

2.10. Estimation of released cytokines

The cytokines such as IL-1β, TNF-α, GMCSF and IL-10 secreted by the cells in the media were quantified by human specific Custom ELISArray, Qiagen. as per manufacture's protocol. The color intensity obtained at the end was measured at an absorbance wavelength of 450 nm using H1 synergy multimode reader.

2.11. In-vitro osteogenesis

MSCs between 3 and 5 passages were used for setting up all the experiments. MSCs revived from the cryogenic conditions were subculture twice, before using for the experiments. MSCs were trypsinized from the maintenance flasks and resuspended in the HiMesoXL™ MSC expansion medium. Nearly 5×10^4 cells in 200 μl of media were seeded on each sample and kept in incubator for 6 h to allow the cell attachment. Afterwards, 800 μl more media was added, and the cells were cultured for 17 days prior to experiments. Media was replaced on every alternate day.

2.11.1. Cell attachment and morphological study

To assess attachment of MSC on the nanofibrous scaffolds and morphological observations, SEM was performed after culturing the cells for 17 days. Samples were then processed for SEM as mentioned in Section 2.3.

2.11.2. Cell viability and proliferation study

Viability and proliferation of MSCs was investigated by Live/dead® staining (Molecular Probes, Invitrogen, USA) and alamar blue assay, respectively. For cell viability, MSCs grown on different fibrous scaffolds were treated for 45 min using 2 μM calcein AM and 4 μM EthD-1 at RT. reated with 0.1% saponin were used as a positive control. All samples were observed under a fluorescent microscope (Axio scope A1; Zeiss, Germany).

Cellular proliferation was quantified using alamar blue assay. The color change is proportional to the number of cells. After 7 days and 17 days of cell culture, 0.15 mg ml^{-1} alamar blue solution was added into each sample at a ratio of 10% volume of cell culture medium. The samples were incubated at 37 °C for 2 h and absorbance was then measured at 570 nm using a multiplate reader.

2.11.3. Alkaline phosphatase (ALP) activity estimation

The osteogenic differentiation was determined by ALP activity as described in our previous studies [13,20]. After 7 days and 17 days of cell culture, media was aspirated out from the fibrous scaffolds and washed with PBS. This was followed by incubating the scaffolds with 800 μl of substrate buffer (0.1 M glycine, pH 10.4 with 1 mM $MgCl_2$ and 1 mM $ZnCl_2$) containing 2 mg ml^{-1} pNPP for 30 min at RT. 2 N NaOH (200 μl) was used to terminate the reaction and the absorbance was read at 405 nm using a multiplate reader. Graph Pad Prism 9.4.1 software was used for plotting the spectral values after normalizing with the corresponding cell number.

2.11.4. Estimation of mineral deposition by alizarin red s staining

Alizarin red s stain selectively binds to hydroxyapatite formed during osteogenic differentiation. This stain quantifies the mineral deposition caused due to osteogenic differentiation of MSCs. Briefly, media was aspirated, and scaffolds were washed with PBS. The washed scaffolds were incubated with 1% alizarin red solution at RT for 30 min, additional wash using water was done to remove excess stain. Finally, the scaffolds were observed under light microscope (Primovert, Zeiss, Germany). Afterwards, scaffolds were air-dried and incubated overnight at room temperature in 10% acetic acid. The extract was heated for 10 min at 85 °C, and brisk cooled on ice for 5 min. The insoluble fractions were pellet down by centrifuged at 20,000 g for 15 min. The supernatant was collected and adjusted to pH 4.1 using 10% NH_4OH. Finally, 200 μL of supernatant was taken for absorbance measurement at 405 nm in a multiplate reader.

2.11.5. Quantification of protein expression by immunocytochemistry

For protein expression study, immunocytochemistry was carried out as reported previously [13]. The fibrous scaffolds containing cells were washed with PBS and fixed with 2% paraformaldehyde for 30 min at RT. Cells were permeabilized with 0.5% Triton X and incubated in blocking solution containing 0.5% bovine serum albumin and 0.15% glycine in 1X PBS for 1 h. The Cy3 conjugated primary antibody for RUNX2 and osteocalcin (with 1:200 dilution) was added to cells for overnight at 4 °C followed by 30 min incubation with nuclear stain DAPI (1 μg/mL) and polyvinyl alcohol mounting medium with DABCO®, antifading. The scaffolds were observed under florescence microscope (Olympus BX53 model, Tokyo, Japan).

2.12. Statistical analysis

All experiments were performed in triplicates (n = 3). The results obtained are depicted as mean ± SEM. The results were analyzed using student's t-test (unpaired with Welch's correction) to determine the significance varying between different scaffold groups using graph-pad prism version 9.4.1 software. A p-value <0.05 was taken to be statistically significant.

3. Results

3.1. Characterizations

The morphological analysis by SEM (Fig. 1a) exhibits the bead free, isotropic, and randomly oriented non-woven fibrous scaffold. The fiber

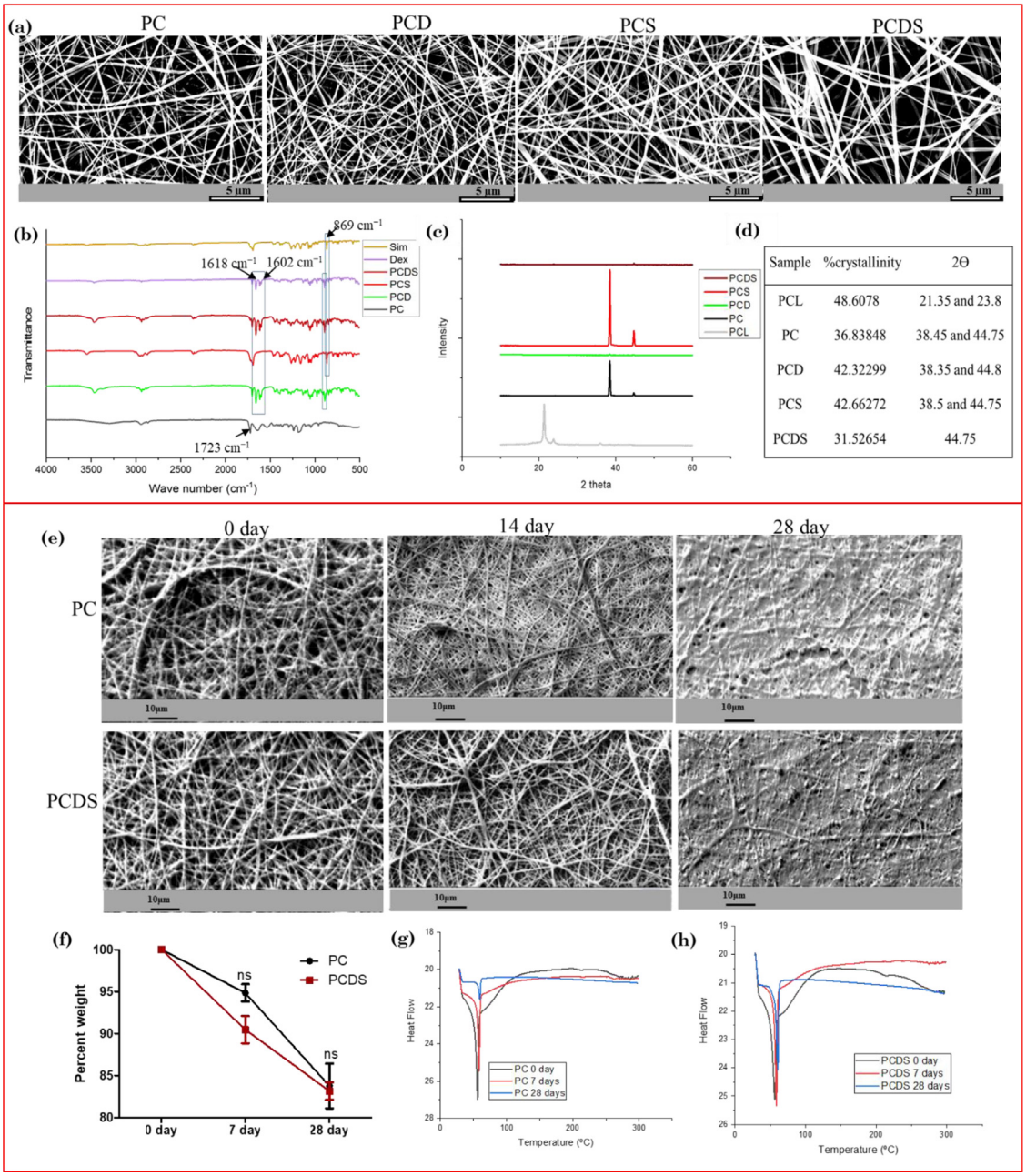

Fig. 1. Physico-chemical characterizations and degradation of fibrous scaffolds: (a) Representative SEM images of PC, PCD, PCS and PCDS scaffolds (scale bar = 5 µm) (b) FTIR spectra of different fibrous scaffolds and the pure drugs, the characteristic peaks are shown by arrows (c) diffractogram of PCL film and fibrous scaffolds (d) and their respective percentage crystallinity and 2Θ. (e) Representative SEM images of PC and PCDS at 0, 7th and 28th day of degradation in PBS (n = 5, scale bar = 10 µm). (f) Percent weight loss of PC and PCDS. DSC thermograph indicating the heat flow (W/g) of PC samples (g), PCDS samples (h) and at 0, 7th and 28th day of degradation in PBS. Bars in graph represents the mean±SEM (n = 5).

diameter distribution was 268 nm to 656 nm for PC, 169 nm to 984 nm for PCD, 231 nm to 892 nm for PCS and 277 nm to 980 nm for PCDS. The mean fiber diameter increased with incorporation of drugs.

The exposure of cell adhesive domains determines the bioactivity of collagen on the fibrous scaffolds. Therefore, surface chemistry of fibrous scaffolds were analyzed by ATR-FTIR analysis. The collagen characteristic peaks at 1640 cm^{-1} and 1540 cm^{-1} for amide I and amide II were observed in all collagen containing samples. The spectrum also shows the characteristic peak of PCL at 1723 cm^{-1} for carbonyl. The characteristic peaks of C–O stretching for dexamethasone are visible in PCD and PCDS at 1602 cm^{-1} and 1618 cm^{-1}. PCS and PCDS also shows the characteristic peaks of simvastatin at 869 cm^{-1}. These characteristic peaks demonstrate the incorporation of dexamethasone in PCD and PCDS; and incorporation of simvastatin in PCS and PCDS.

The results of wide angle XRD analysis are shown in Fig. 1(c) and (d) which depict that crystallinity of PCL is reduced due to addition of collagen during electrospinning process. The crystallinity of pristine PCL film was found to be ~48.6%, which was reduced to ~36% in PC. The crystallinity of single drug loaded fibers (PCD and PCS) was found to be ~42%. However, it was reduced to ~32% in the dual drug loaded fibers. The reduced crystallinity was also confirmed by the change in diffractogram peaks at 2Θ. The 2Θ peaks for PCL was observed at 21.35 and 23.8, which confirms the crystalline nature of PCL However, these peaks had shifted to around 38.45 and 44.75 in the fibrous scaffolds,

respectively, which again demonstrated the effect of electrospinning and drug loading in crystallinity of PCL

The crystallinity also influences the degradation of scaffolds, which was considered to study the behavior of fibrous scaffolds. Fig. 1(e) shows the SEM images, which depicts that scaffold integrity was retained up to 28 days. Two-fold increase in fiber diameter from 494 ± 357 nm to 916 ± 473 nm in PC and 579 ± 406 nm to 1002 ± 573 nm in PCDS scaffolds demonstrate the swelling of fibers and chain relaxation of polymer. The swelling could allow the release of loaded molecules and adsorption of protein in media. However, at later time point (28th day) the surface erosion became prominent and created a thin film like morphology. The change in fiber morphology was also confirmed by weight loss study shown in Fig. 1(f). At 7th day, 5.1 and 9.5% weight loss were found in PC and PCDS, respectively. This could be due to swelling followed by loss of uncross linked polymer chains. At 28th day, 16.2 and 16.8% weight loss were found in PC and PCDS, respectively. Change in crystallinity could also influence the degradation behavior of polymeric scaffolds. Therefore, DSC analysis was carried out which demonstrated 26.96 W/g (heat flow) in PC samples before degradation, it was progressively decreased to 25.44 W/g at 7th day and 21.62 W/g at 28th day (Fig. 1(g)). On the other hand, maximum peak height of PCDS was observed at 25.11 W/g at 0 day, which progressively declined to 24.07 W/g at 28th day of degradation (Fig. 1(h)). The results demonstrated 5.34 W/g and 1.04 W/g reduction in heat flow of PC and PCDS, respectively from 0 day to 28th day of degradation.

3.2. Inflammatory study

3.2.1. Dual drug releasing fibrous scaffolds retained the morphological features of monocytes and influences nitric oxide release

The anti-inflammatory role of these nanofibrous scaffolds were studied by using U937 cells. Due to the inflammatory response, round shaped, suspension monocytes are differentiated into adherent macrophages, which are characterized by the presence of phillopodia and lamellipodia like structures. The SEM has been performed to study the morphological changes induced in monocytes on TCPS, PC, PCD, PCS, PCDS and TCPS+PMA (Fig. 2(a)). TCPS acts as control in the experiment, no morphological change was observed in cells grown on TCPS. The cells show the round shape with 0.909 average circularity, 8340 area and 1.07 aspect ratio. On PC, the average circularity of cells was reduced to 0.443, area was increased to 19,071 and the aspect ratio was increased to 1.27. On PCS also, cells showed some inclination towards macrophage phenotype (Fig. 2(b)). The circularity was 0.731, area 6706 and aspect ratio was 1.2. On PCD, the cells showed 0.9 circularity, 3845 area and 1.2 aspect ratio. Cells on PCDS also showed more circularity and lesser aspect ratio. The circularity was 0.888, area 3244 and aspect ratio was 1.186 (Fig. 2(b)). The cells treated with PMA showed lesser circularity and more aspect ratio, which indicated that the cells are differentiated into macrophages. The circularity was 0.381, area 30,609 and aspect ratio 1.452. The result (Fig. 2(c)) also demonstrated that the cells treated with PMA produced significantly higher levels of NO, followed by cells grown on PC. In comparison to PC the NO levels reduced to 0.7-, 0.8- and 0.5-fold ($p<0.005$) in PCD, PCS and PCDS groups, respectively. PMA stimulation was used as a positive control in this model, where PMA is observed to induce significant levels of NO.

3.2.2. Dual drug-loaded fibrous scaffold promotes an anti-inflammatory gene expression

To understand the effect of scaffolds on monocyte differentiation to macrophage and their polarization at the molecular level, we analyzed the expression of certain critical pro-inflammatory genes such as TNF-α, IL-1β, GMCSF and anti-inflammatory gene such as IL-10. Transcriptional levels of these genes were examined using qPCR with GAPDH used as the loading control (Fig. 2(d)). The mRNA expression of TNF-α, IL-1β and GMCSF increased by 5.7-, 2.9-, 4.3- fold ($p<0.05$) in cells cultured in PC group compared to the control group. In comparison to the PC group, in PCD group TNF-α, IL-1β and GM-CSF decreased to 0.3-, 0.3- and 0.4- fold, respectively; in PCS group they reduced to 0.8-, 0.5- and 0.3- -fold, respectively and in PCDS group their levels depreciated to 0.2-, 0.3- and 0.2- fold, respectively. PCD effectively reduced the expression of inflammatory markers, which further reduced in PCDS group in comparison to PC group. PCS group was effective in reducing the expression of IL-1β and GMCSF. In addition, we also analyzed the expression of an important anti-inflammatory cytokine, widely known to be expressed by M2-macrophages. The expression of IL-10 increased by 1.3-fold in PCDS group in comparison to PC group. However, the PCD and PCS group did not have any significant difference in the expression of IL-10 in comparison to the PC group.

Innate immune cells release an array of cytokines and chemokines. The specific type of cytokines released by macrophages are important in characterizing the differentiation and polarization of the macrophages into the proinflammatory (M1) and anti-inflammatory (M2) type. The cytokine such as IL-1β, TNF-α, GMCSF and IL-10 were confirmed using ELISA (Fig. 2(e)). In accordance with the morphological and transcriptional studies of critical pro and anti-inflammatory genes, the cytokine levels were analyzed. In PMA induced group elevated levels of proinflammatory cytokines was observed. In comparison to PC group the levels of TNF-α reduced to 0.7-, 0.6- and 0.5-fold; IL-1β reduced to 0.9-, 0.8- and 0.8-fold; GMCSF reduced to 0.8-, 0.7- and 0.65-fold in PCD, PCS and PCDS groups, respectively in comparison to PC group. However, not much difference was observed in IL-10 levels.

3.3. Osteogenic study

3.3.1. Dual drug releasing fibrous scaffolds induced the osteogenesis of MSCs by increasing mineral deposition

The morphology of MSCs grown on different fibrous scaffolds were observed by SEM. The results (Fig. 3(a) upper panel) demonstrated that uniform cell adhesion and spreading across the surfaces. The MSCs were allowed to grow until day 17, where spindle shaped and flat morphology was observed on fibrous scaffolds and TCPS surface, respectively. The viability of MSCs was studied by performing Live/Dead® staining assay (Fig. 3(a) middle and lower panel). Calcein AM in this assay gives green fluorescence when taken up by the live cells due to their esterase activity; whereas ethidium homodimer-1 binds to DNA via rupture cell membrane and produce red fluorescence in dead cells. The red florescence indicates the dead cells, which was observed in control group, where cells were treated with saponin. However, the cells grown on different fibrous scaffolds showed green florescence, which indicates live cells and confirms the cytocompatibility of fibrous scaffolds for MSCs. Subsequently, cell growth was measured using alamar blue assay, which is a nondestructive and reusable method to examine the parameters of viability, proliferation and metabolic activity of the cells. The results demonstrated that there is no significant difference in the proliferation of MSCs on PC, PCD, PCS and PCDS at 7 days and 17 days. However, there was significantly higher cell growth at 17 days as compared to 7 days on all the fibrous scaffolds (Fig. 3(b)), indicating the cell proliferation on fibrous scaffolds.

During osteogenic differentiation of stem cells, mineral deposition has a prime role in maturation of osteoblasts. The hydrolysis of the phosphate esters by ALP increases the concentration of phosphate in ECM. Figure S1 and Fig. 3(c) shows the ALP activity of MSCs on PC, PCD, PCS and PCDS. There was no significant difference in ALP activity on any of the scaffold after 7 days. Again after 17 days, there was no significant difference in ALP activity of cells on PCS as compared to PC, however, significant increase in ALP activity was observed on PCD ($p = 0.0040$), which was further increased on PCDS ($p = 0.0002$). The mineral deposits are stained red by Alizarin red s stain and indicated for osteogenic differentiation of stem cells. Fig. 3(d) shows the mineral deposition by MSCs. As compared to PC, 1.6-, 1.3- and 1.86-fold increased mineral deposition was observed on PCD, PCS and PCDS, respectively. The representative images (Fig. 3(e)) also demonstrate increased mineral deposition

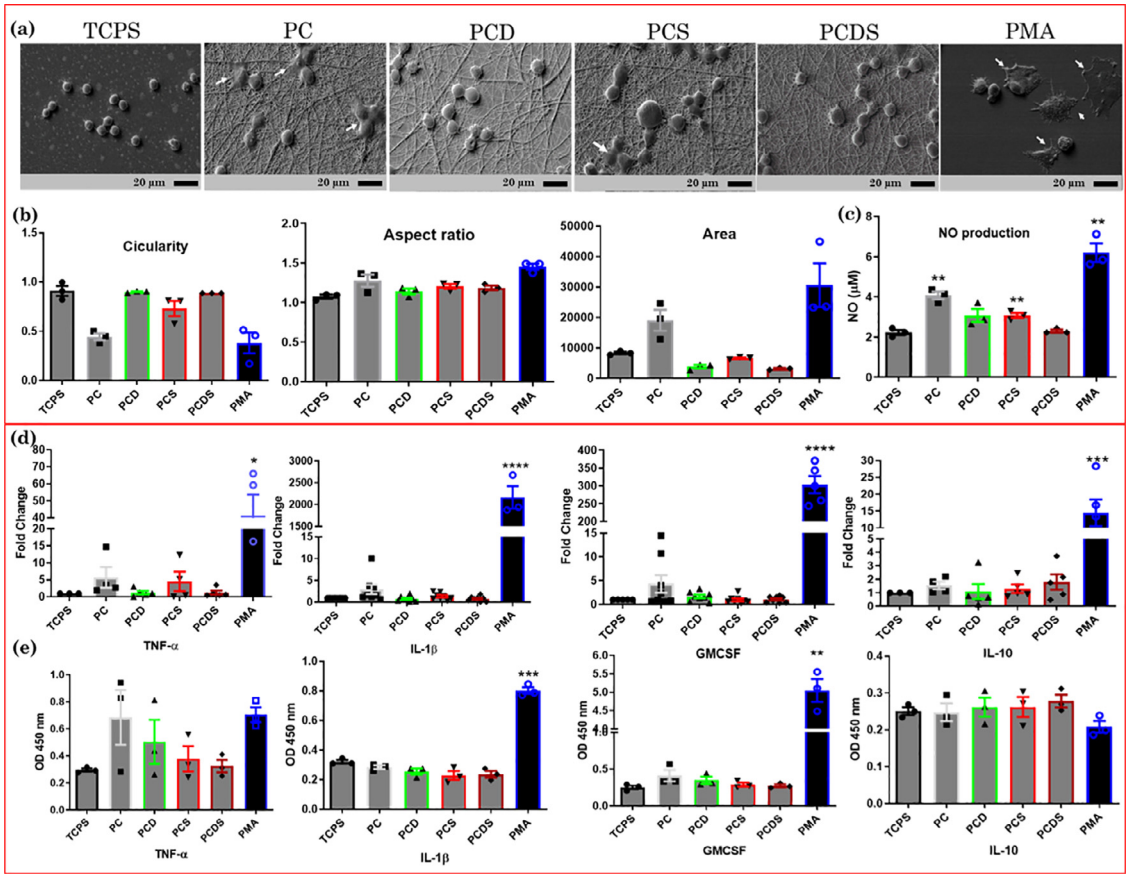

Fig. 2. Morphological changes, gene expression and cytokine levels of U937 cells; (a) Representative SEM images of U937 cells cultured on TCPS, PC, PCD, PCS, PCDS and TCPS+PMA after 48 h of seeding (scale bar = 20 µm). (b) Histograms represent the circularity, aspect ratio and area of cells, respectively (n = 3). (c) Histograms of NO production from U937 cells by Griess reagent on TCPS, PC, PCD, PCS, PCDS and TCPS+PMA (n = 3). (d) Histograms represent the level of gene expression by U937 cells and (e) level of cytokines secreted by monocytes cultured on different scaffolds after 48 h (n = 3).

on PCD, PCS and PCDS as compared to PC. Among drug loaded fibrous scaffolds PCDS demonstrated the highest mineral deposition followed by PCD and PCS. The calcium deposition was further analyzed by EDX analysis. TCPS was taken as control, which did not show any calcium deposition (Fig. 3(f)). PC showed 0.42 mass% and 0.14 atom%, PCD showed 2.67 mass% and 0.95 atom%, PCS 2.54 mass% and 0.91 atom%, and PCDS 3.35 mass% and 1.17 atom%. These results further support the alizarin red staining results, which indicates the role of dual drug releasing fibers in mineral deposition during osteogenic differentiation of MSCs.

3.3.2. Dual drug releasing fibrous scaffolds induced the osteogenesis of MSCs by increasing the mRNA and protein expression RUNX2 and osteocalcin

The osteogenic effect was further studied at molecular level by performing semi-quantitative RTPCR to analyze expression of osteogenic genes RUNX2 and osteocalcin. Fig. 4(a) shows the representative bands for RUNX2, osteocalcin and GAPDH mRNA expression after 17 days of cell culture. PCD, PCS and PCDS demonstrated significant increase in mRNA expression as compared to PC. In case of PCD, the RUNX2 and osteocalcin expression was 1.7-fold increased. Although, PCS shows only 1.1-fold increase of osteocalcin expression, it exhibited 1.6-fold increase in RUNX2 mRNA expression. PCDS exhibited 3.4-fold and 1.9-fold increase in RUNX2 and osteocalcin expressions, respectively.

The osteoinductive potential was further quantified by the immunofluorescence staining of RUNX2 and osteocalcin after 17 days of MSC culture (Fig. 4(b)). PC showed the least expression of RUNX2 as well as osteocalcin. Cells grown on PCD, PCS and PCDS exhibited higher expression of RUNX2 as well as osteocalcin than on PC. The corrected total cell fluorescence (Fig. 4(c) and (d)) demonstrated lowest expression of RUNX2 and osteocalcin on PC. Cells grown on PCD showed second highest level of expression for RUNX2 (p = 0.0227) and osteocalcin (p = 0.0439), those on PCS did not show much increase in expression of RUNX2 (p = 0.124) or osteocalcin (p = 0.11). MSCs grown on PCDS demonstrated significantly higher expression of RUNX2 (p = 0.0011), which was 2.2-fold and of osteocalcin expression, which was 8.3-fold (p < 0.0001) higher as compared to PC. These results are in corroboration with the mRNA expression results, which further confirms the role of dual drug releasing fibrous scaffolds to induce osteogenesis of MSCs.

4. Discussion

To mimic the natural architecture of bone ECM, we have developed PCL-collagen nanofibrous scaffolds utilizing HFIP as a solvent system. PCL is an FDA approved implantable polymer, which can be functionalized as an osteoconductive substrate by adding certain biopolymers during electrospinning process, including collagen [11–13]. Dexamethasone and simvastatin were used to further synergize the osteoinductive feature and immunocompatability [14–16]. HFIP plays a pivotal role in emulsion electrospining due to its high relative dielectric permittivity values (17.8). Which ensures strong polar interactions between protein and PCL chains. Further, HFIP promotes higher net charge density in polymeric solution, which enhances bending instability, jet path and enhanced stretching of fibers resulting in thinner fibers [21]. The overall diameter distribution range demonstrates the resemblance with collagen fibrils of bone [22]. It demonstrates that the fibrous scaffolds mimic

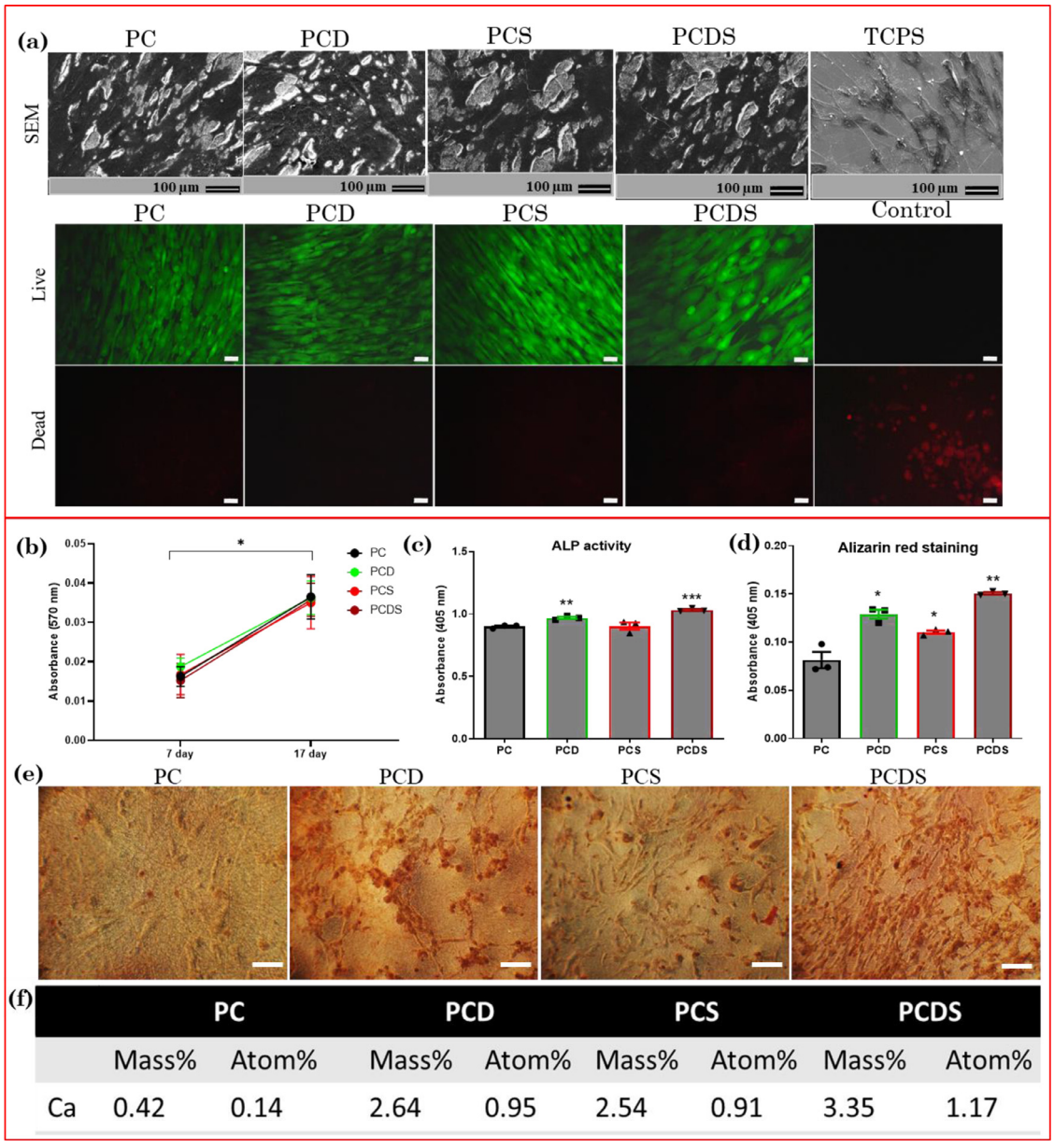

Fig. 3. (a) Upper panel shows representative SEM images of MSCs after 17 days (scale bar = 100 μm), middle and lower panel shows live and dead cells, respectively (scale bar = 50 μm). (b) cell proliferation measured by alamar blue assay, (c) Alkaline phosphatase activity, (d) alizarin red s stain quantification, (e) representative bright field images of alizarin red s staining (scale bar = 200 μm) and (f) calcium deposition during osteogenic differentiation of MSCs on different scaffolds after 17 days performed by EDX analysis. All experiments were performed in triplicates (n = 3) and results were plotted as mean ±SEM.

the architecture of bone ECM. The surface chemistry demonstrates the exposure of PCL and collagen, which could strengthen the cell adhesion. Furthermore, characteristic peaks of dexamethasone and simvastatin demonstrates their readily availability for cells. The similar results were observed in our previous study by X-ray photon spectroscopy analysis [13].

In polymeric scaffold, the crystallinity of constituent polymers influences the overall biocompatibility of the scaffold. It is reported that reduction in the crystallinity of PCL during electrospinning process enhances the cell attachment and proliferation on the nanofibrous scaffolds [23,24]. It could be because of fast solvent evaporation, which provides less opportunity for PCL to rearrange molecular chains, nucleate and crystallize [25,26]. Furthermore, incorporation of amorphous collagen in PCL solution could decrease the crystallinity of the scaffolds [27]. The embedding of amorphous protein in the PCL matrix could lead to significant amorphization, thereby disrupting the crystalline regions [28]. The crystallinity of polymeric scaffolds could influence their degradation at physiological condition, which is important to determine their biodegradability and bioactivity. S.-H. Park et al. demonstrated that scaffold degradation rates directly impact the metabolism of hMSCs and rate of osteogenesis [29]. The surface integrity was retained up to 28 days. Two-fold increase in fiber diameter demonstrate the swelling of fibers and chain relaxation of polymer. The swelling could allow the release of loaded molecules, which is evident in our previous study [13]. However, at later time point (28th day) the surface erosion became prominent and created a thin film like morphology. The reason could be the conglutination of fibers due to their swelling in aqueous media [30]. The reduction of heat flow could be because of the changes in PCL microstructure [23]. PC showed much reduction, which could be due to hydrolysis of ester linkages in PCL [31]. On the other hand, lesser reduction in heat flow of PCDS samples could be because of more surface exposure of collagen, which could cause less hydrolysis of PCL. The

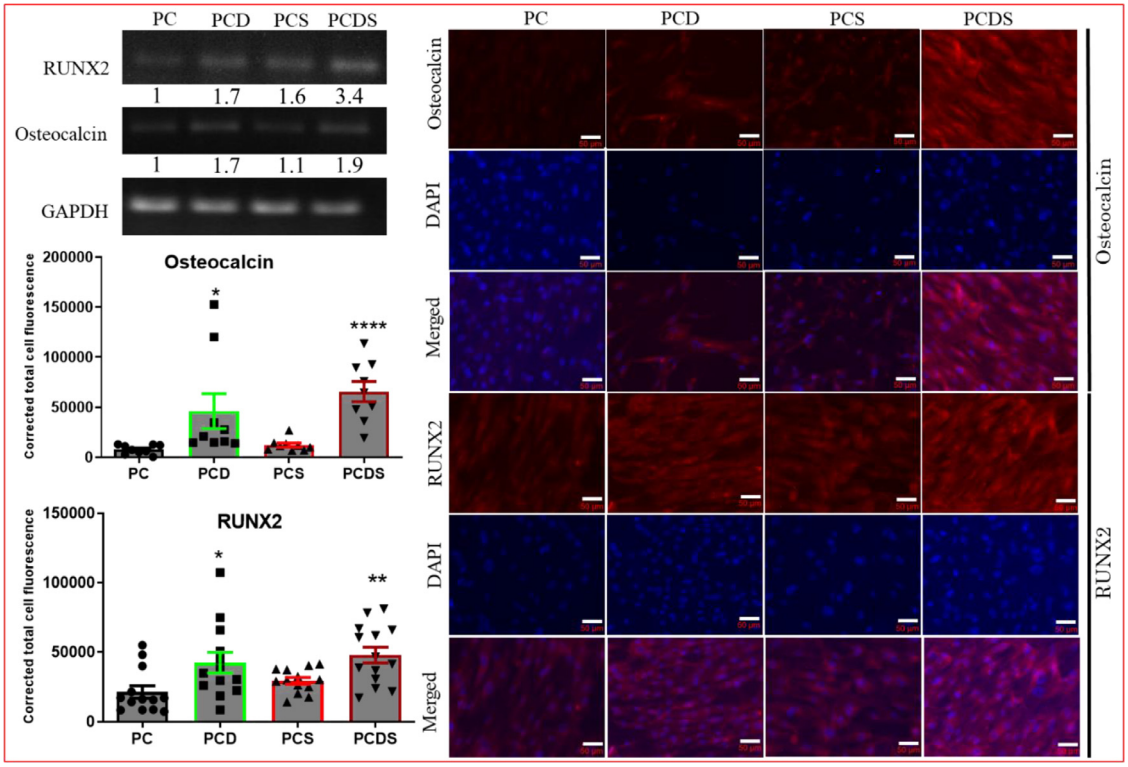

Fig. 4. Osteogenic gene and protein expression in MSCs: (a) the representative images of RUNX2 and Osteocalcin mRNA expression and (b) immunofluorescence images of MSCs after 17 days of cell culture on PC, PDC, PCS and PCDS, respectively (n = 3), red fluorescence indicates the expression of RUNX2 and OC in the respective images and blue fluorescence indicates nuclear stained by DAPI. (c and d) RUNX2 and OC graphical represented based on the corrected total cell florescence of IF images (n = 13). Scale bar = 50 μm.

overall results demonstrate that the fiber integrity was retained up to 28th day and hence these fibrous scaffolds could be used for prolonged *in vitro* and *in vivo* studies.

The inflammatory response of these scaffolds were studied by using U937 cells. Changes in the morphological features of monocytes and their molecular profile was characterized. More circularity, lesser area and lesser aspect ratio means that the cells are round, which is the characteristic feature of monocytes. PC showed some inclination towards transformation of monocytes into macrophages, the reason could be the triggered immune response which could lead to monocyte differentiation into macrophages [32]. PMA is a chemical inducer of monocyte differentiation into macrophage. The cells treated with PMA showed lesser circularity and more aspect ratio, which indicated that the cells are differentiated into macrophages. In dual drug releasing scaffold, monocytes maintained their spherical morphology as observed in TCPS, demonstrating their anti-inflammatory features. Monocytes and macrophages could produce basal levels of nitric oxide (NO), which has been identified as an important regulator as well as a mediator of varied signaling transduction pathways. However, in presence of certain inducers the cells tend to produce higher level of NO due to activation of inducible nitric oxide synthase (iNOS), expressed by M1 macrophages [33]. NO via modulating several signaling pathways can elevate the production of TNF-α, IFN-γ, IL-6 and IL-1β in immune cells [34]. The increased levels of NO production in PC could be attributed to differentiation of monocytes into M1 macrophages, which was observed to decrease appreciably in the PCDS group. Presence of dexamethasone and simvastatin in the fibrous scaffold had an additive effect in reducing NO production and indicates the anti-inflammatory effect.

Scaffolds used for tissue regeneration have long known to induce a host inflammatory response by the release of multiple factors including transforming growth factor alpha (TGF-α), platelet factor 4 (PF4), and platelet-derived endothelial cell growth factor (ECGF1) and these agents augment monocyte chemotaxis and differentiation into M1 macrophages [35]. Macrophages recognize several damage associated molecular patterns followed by activation of several TLRs and inflammasome which mediates the activation and elevated expression of TNF-α and IL-1β, respectively [36,37]. These cytokines have both autocrine and paracrine effects and aggravate the inflammatory microenvironment. GM-CSF is a recent addition in the profile of cytokines manifested by M1 macrophages. GM-CSF contributes towards antigen presentation, phagocytosis leukocyte chemotaxis and adhesion. In addition, it also induces monocytes and macrophages to produce an array of cytokines such as IL-6, G-CSF, M-CSF, TNF-α, IL-1β and IL-8 [36]. Release of dexamethasone reduced the expression of inflammatory markers and increased expression of anti-inflammatory marker and their secretion. Furthermore, supplementing it with simvastatin enhances the effectiveness of reducing inflammatory microenvironment, indicating their role in reducing the pro-inflammatory markers which are manifested in monocytes and macrophages skewed to the M1 type. The anti-inflammatory microenvironment creates a niche which is beneficial and propels wound healing properties.

Adipose-derived MSCs have several advantages including availability, and ease of harvesting. MSCs possess immunomodulatory characteristics because MHC class II is not expressed and low levels of MHC I are expressed [38]. Furthermore, MSCs are most viable candidates for bone regeneration because of their osteogenic differentiation potential. Hence, MSCs were utilized for studying the osteogenic potential of the drug loaded fibrous scaffolds. The proliferation rate of MSCs were not altered on the nanofibrous scaffolds. The possible reason could be that all scaffolds possess equal proportion of collagen, which provides cell adhesion sites, which in turn could result in equal cell proliferation. During osteogenic differentiation of stem cells, mineral deposition has a prime role in maturation of osteoblasts. The hydrolysis of the phosphate esters by ALP increases the concentration of phosphate in ECM.

Therefore, it is considered as primary marker for osteogenic differentiation [23]. Further, staining of hydroxyapatite formation is used as a parameter for osteogenesis differentiation [39]. Highest ALP activity and mineral deposition was observed on PCDS followed by PCD and PCS. The reason could be the presence of dexamethasone in these scaffolds, because it is a key ingredient of osteogenic differentiation media and enhances the hydroxyapatite formation [40,41]; hence it might have more osteo inducing potential as compared to simvastatin. Simvastatin has positive effects on osteogenic differentiation, however it is reported that simvastatin increases the expression of collagen I and RUNX2 during osteogenesis but did not increase ALP activity and alizarin red s staining [42]. The calcium deposition analyzed by EDX further support the alizarin red staining results, which indicates the role of dual drug releasing fibers in mineral deposition during osteogenic differentiation of MSCs. RUNX2 acts as a transcription factor which is majorly active during initial stages of osteogenic differentiation, and osteocalcin is the major non-collagen ECM protein, which is expressed during the middle and later stages [43,44]. The higher expression of RUNX2 and osteocalcin on PCDS could be anticipated for synergistic effect of dual drugs. The overall mRNA expression profile suggested osteoinductive effect of dual drugs in MSCs. These results are in corroboration with the protein expression results, which further confirms the role of dual drug releasing fibrous scaffolds to induce osteogenesis of MSCs.

5. Conclusion

Monocytes differentiating into M1 type of macrophages in a pro-inflammatory niche is a common phenomenon associated with delayed wound healing and osteogenesis. Macrophages in the presence of endogenous stressors tend to release inflammatory cytokines which has an autocrine and paracrine effect on the cells in its vicinity. Inflammatory response generated in association with biomaterial scaffolds is generally due to unfavorable microenvironment, making the implant susceptible to an inflammatory response. Therefore, delivery of anti-inflammatory drugs such as dexamethasone promotes the polarization of macrophages towards the M2 phenotype (anti-inflammatory) suppressing the inflammation associated pathways. In this study, encapsulation of dexamethasone and simvastatin was intended to modulate the host inflammatory response towards these scaffolds and induce osteogenic differentiation. The NO level, inflammatory gene expression and cytokine analysis indicated that M2 polarization was favored in the presence of dual drugs. Among drug loaded scaffolds, dexamethasone releasing scaffolds (PCD and PCDS) demonstrated more anti-inflammatory properties as compared to simvastatin alone loaded scaffold (PCS) due to anti-inflammatory potential of dexamethasone. The mineral deposition, gene expression and protein expression demonstrated the osteogenic differentiation of MSCs. Furthermore, PCDS demonstrated synergistic effect on osteogenic differentiation of MSCs. Thus, the dual drug loaded fibrous scaffolds has immunomodulatory function and enhances osteogenesis and hence could be used for bone tissue engineering applications.

Declaration of competing interest

Authors declare no conflict of interest for manuscript titled “Polycaprolactone-collagen nanofibers loaded with dexamethasone and simvastatin as osteoinductive and immunocompatible scaffold for bone regeneration applications”

Data Availability

Data will be made available on request.

Acknowledgements

The work was supported and funded by DST, Nanomission, Govt. of India project grant (No. SR/NM/NB-1079/2017(G)). Senior Research Fellowship (SRF) to HR from DST, Nanomission and to JFV from Gujarat State Biotechnology Mission (GSBTM), Govt. of Gujarat and award of Ramanujan fellowship by SERB/DST to UCSY are thankfully acknowledged. BD would like to be acknowledged to Council of Scientific and Industrial Research, Junior Research Fellowship for financial support. We also thank Flair Labs, Surat, India for providing rat tails for collagen isolation.

Supplementary materials

Supplementary material associated with this article can be found, in the online version, at doi:10.1016/j.bbiosy.2022.100064.

References

[1] Seo BB, Choi H, Koh JT, Song SC. Sustained BMP-2 delivery and injectable bone regeneration using thermosensitive polymeric nanoparticle hydrogel bearing dual interactions with BMP-2. J Control Release 2015;209:67–76.
[2] Zhang B, Su Y, Zhou J, Zheng Y, Zhu D. Toward a better regeneration through implant-mediated immunomodulation: harnessing the immune responses. Adv Sci (Weinh) 2021;8(16):e2100446.
[3] Zhao B, Katagiri T, Toyoda H, Takada T, Yanai T, Fukuda T, Chung UI, Koike T, Takaoka K, Kamijo R. Heparin potentiates the in vivo ectopic bone formation induced by bone morphogenetic protein-2. J Biol Chem 2006;281(32):23246–53.
[4] Josephson AM, Bradaschia-Correa V, Lee S, Leclerc K, Patel KS, Muinos Lopez E, Litwa HP, Neibart SS, Kadiyala M, Wong MZ, Mizrahi MM, Yim NL, Ramme AJ, Egol KA, Leucht P. Age-related inflammation triggers skeletal stem/progenitor cell dysfunction. Proceedings of the Nat Acad Sci 2019;116(14):6995–7004.
[5] He J, Chen G, Liu M, Xu Z, Chen H, Yang L, Lv Y. Scaffold strategies for modulating immune microenvironment during bone regeneration. Mater Sci Eng C Mater Biol Appl 2020;108:110411.
[6] Schlundt C, El Khassawna T, Serra A, Dienelt A, Wendler S, Schell H, van Rooijen N, Radbruch A, Lucius R, Hartmann S, Duda GN, Schmidt-Bleek K. Macrophages in bone fracture healing: their essential role in endochondral ossification. Bone 2018;106:78–89.
[7] Dai X, Heng BC, Bai Y, You F, Sun X, Li Y, Tang Z, Xu M, Zhang X, Deng X. Restoration of electrical microenvironment enhances bone regeneration under diabetic conditions by modulating macrophage polarization. Bioact Mater 2021;6(7):2029–38.
[8] Mahon OR, Browe DC, Gonzalez-Fernandez T, Pitacco P, Whelan IT, Von Euw S, Hobbs C, Nicolosi V, Cunningham KT, Mills KHG, Kelly DJ, Dunne A. Nano-particle mediated M2 macrophage polarization enhances bone formation and MSC osteogenesis in an IL-10 dependent manner. Biomaterials 2020;239:119833.
[9] Rowley AT, Nagalla RR, Wang S-W, Liu WF. Extracellular matrix-based strategies for immunomodulatory biomaterials engineering. Adv Healthc Mater 2019;8(8):1801578.
[10] Holländer J, Genina N, Jukarainen H, Khajeheian M, Rosling A, Mäkilä E, Sandler N. Three-dimensional printed pcl-based implantable prototypes of medical devices for controlled drug delivery. J Pharm Sci 2016;105(9):2665–76.
[11] Jhala D, Rather HA, Vasita R. Extracellular matrix mimicking polycaprolactone–chitosan nanofibers promote stemness maintenance of mesenchymal stem cells via spheroid formation. Biomed Mater 2020;15(3):035011.
[12] Ren K, Wang Y, Sun T, Yue W, Zhang H. Electrospun PCL/gelatin composite nanofiber structures for effective guided bone regeneration membranes. Mater Sci Eng C Mater Biol Appl 2017;78:324–32.
[13] Rather HA, Patel R, Yadav UCS, Vasita R. Dual drug-delivering polycaprolactone-collagen scaffold to induce early osteogenic differentiation and coupled angiogenesis. Biomed Mater 2020;15(4):045008.
[14] Jiang K, Weaver JD, Li Y, Chen X, Liang J, Stabler CL. Local release of dexamethasone from macroporous scaffolds accelerates islet transplant engraftment by promotion of anti-inflammatory M2 macrophages. Biomaterials 2017;114:71–81.
[15] Yuasa M, Yamada T, Taniyama T, Masaoka T, Xuetao W, Yoshii T, Horie M, Yasuda H, Uemura T, Okawa A, Sotome S. Dexamethasone enhances osteogenic differentiation of bone marrow- and muscle-derived stromal cells and augments ectopic bone formation induced by bone morphogenetic protein-2. PLoS ONE 2015;10(2):e0116462.
[16] Gentile P, Nandagiri VK, Daly J, Chiono V, Mattu C, Tonda-Turo C, Ciardelli G, Ramtoola Z. Localised controlled release of simvastatin from porous chitosan–gelatin scaffolds engrafted with simvastatin loaded PLGA-microparticles for bone tissue engineering application. Mater Sci Eng: C 2016;59:249–57.
[17] Zhang M, Bian YQ, Tao HM, Yang XF, Mu WD. Simvastatin induces osteogenic differentiation of MSCs via Wnt/β-catenin pathway to promote fracture healing. Eur Rev Med Pharmacol Sci 2018;22(9):2896–905.
[18] Rajan N, Habermehl J, Coté MF, Doillon CJ, Mantovani D. Preparation of ready–to-use, storable and reconstituted type I collagen from rat tail tendon for tissue engineering applications. Nat Protoc 2006;1(6):2753–8.
[19] Kedaria D, Vasita R. Bi-functional oxidized dextran–based hydrogel inducing micro-tumors: an in vitro three-dimensional lung tumor model for drug toxicity assays. J Tissue Eng 2017;8:2041731417718391.
[20] Kumar Meena L, Rather H, Kedaria D, Vasita R. Polymeric microgels for bone tissue engineering applications – a review. International J Polymeric Mater Polymeric Biomater 2019:1–17.

[21] Guarino V, Cirillo V, Taddei P, Alvarez-Perez MA, Ambrosio L. Tuning size scale and crystallinity of pcl electrospun fibres via solvent permittivity to address hmsc response. Macromol Biosci 2011;11(12):1694–705.
[22] Rho J-Y, Kuhn-Spearing L, Zioupos P. Mechanical properties and the hierarchical structure of bone. Med Eng Phys 1998;20(2):92–102.
[23] Jhala D, Rather H, Vasita R. Polycaprolactone-chitosan nanofibers influence cell morphology to induce early osteogenic differentiation. Biomater Sci 2016;4(11):1584–95.
[24] Rather HA, Thakore R, Singh R, Jhala D, Singh S, Vasita R. Antioxidative study of Cerium Oxide nanoparticle functionalised PCL-Gelatin electrospun fibers for wound healing application. Bioactive Mater 2018;3(2):201–11.
[25] Wang X, Zhao H, Turng L-S, Li Q. Crystalline Morphology of Electrospun Poly(ε-caprolactone) (PCL) Nanofibers. Ind Eng Chem Res 2013;52(13):4939–49.
[26] Junkasem J, Rujiravanit R, Grady BP, Supaphol P. X-ray diffraction and dynamic mechanical analyses of α-chitin whisker-reinforced poly(vinyl alcohol) nanocomposite nanofibers. Polym Int 2010;59(1):85–91.
[27] Zhang Q, Lv S, Lu J, Jiang S, Lin L. Characterization of polycaprolactone/collagen fibrous scaffolds by electrospinning and their bioactivity. Int J Biol Macromol 2015;76:94–101.
[28] Khan I, Nagarjuna R, Dutta JR, Ganesan R. Enzyme-embedded degradation of poly(ε-caprolactone) using lipase-derived from probiotic lactobacillus plantarum. ACS Omega 2019;4(2):2844–52.
[29] Park S-H, Gil ES, Shi H, Kim HJ, Lee K, Kaplan DL. Relationships between degradability of silk scaffolds and osteogenesis. Biomaterials 2010;31(24):6162–72.
[30] Vasita R, Shanmugam K, Katti DS. Degradation behavior of electrospun microfibers of blends of poly(lactide-co-glycolide) and Pluronic® F-108. Polym Degrad Stab 2010;95(9):1605–13.
[31] Sisson AL, Ekinci D, Lendlein A. The contemporary role of ε-caprolactone chemistry to create advanced polymer architectures. Polymer (Guildf) 2013;54(17):4333–50.
[32] Smith SR, Schaaf K, Rajabalee N, Wagner F, Duverger A, Kutsch O, Sun J. The phosphatase PPM1A controls monocyte-to-macrophage differentiation. Sci Rep 2018;8(1):902.
[33] Ley K. M1 Means Kill; M2 Means Heal. The J Immunol 2017;199(7):2191–3.
[34] Soufli I, Toumi R, Rafa H, Touil-Boukoffa C. Overview of cytokines and nitric oxide involvement in immuno-pathogenesis of inflammatory bowel diseases. World J Gastrointest Pharmacol Ther 2016;7(3):353–60.
[35] Rutledge KE, Cheng Q, Jabbarzadeh E. Modulation of inflammatory response and induction of bone formation based on combinatorial effects of resveratrol. J Nanomed Nanotechnol 2016;7(1):350.
[36] Martinez FO, Gordon S. The M1 and M2 paradigm of macrophage activation: time for reassessment. F1000Prime Rep 2014;6 13-13.
[37] Varghese JF, Patel R, Yadav UCS. Sterol regulatory element binding protein (SREBP) -1 mediates oxidized low-density lipoprotein (oxLDL) induced macrophage foam cell formation through NLRP3 inflammasome activation. Cell Signal. 2019;53:316–26.
[38] Blanc KLe, Tammik C, Rosendahl K, Zetterberg E, Ringdén O. HLA expression and immunologic properties of differentiated and undifferentiated mesenchymal stem cells. Exp Hematol 2003;31(10):890–6.
[39] Meena LK, Rather HA, Vasita R. Single-step fabrication of core–shell microgels for the controlled release of rhbmp-2 and simvastatin to induce osteogenesis. ACS Applied Polymer Materials 2020;2(11):4902–13.
[40] Werner SB, Tessler J, Guglielmotti MB, Cabrini RL. Effect of dexamethasone on osseointegration: a preliminary experimental study. J Oral Implantol 1996;22(3–4):216–19.
[41] Roozegar MA, Mohammadi TM, Havasian MR, Panahi J, Hashemian A, Amraei M, Hoshmand B. In vitro osteogenic impulse effect of dexamethasone on periodontal ligament stem cells. Bioinformation 2015;11(2):96–100.
[42] Lee H, Lee H, Na CB, Park JB. The effects of simvastatin on cellular viability, stemness and osteogenic differentiation using 3-dimensional cultures of stem cells and osteoblast-like cells, Advances in clinical and experimental medicine: official organ. Wroclaw Med Univ 2019;28(5):699–706.
[43] Huang W, Yang S, Shao J, Li Y-P. Signaling and transcriptional regulation in osteoblast commitment and differentiation. Front Biosci 2007;12:3068–92.
[44] Tsao Y-T, Huang Y-J, Wu H-H, Liu Y-A, Liu Y-S, Lee OK. Osteocalcin mediates biomineralization during osteogenic maturation in human mesenchymal stromal cells. Int J Mol Sci 2017;18(1):159.